

## STRUCTURAL AND OPTICAL PROPERTIES OF $\text{Al}_2\text{ZnO}_4$ THIN FILMS DEPOSITED BY DC SPUTTERING TECHNIQUE

H. H. AL-OFI<sup>a</sup>, M. M. ABD EL-RAHEEM<sup>a,b\*</sup>, ATEYYAH M. AL-BARADI<sup>a</sup>, A. A. ATTA<sup>a,c</sup>

<sup>a</sup>*Department of Physics, faculty of science, Taif University, Taif 888, KSA*

<sup>b</sup>*Department of Physics, faculty of science, Sohag University, Sohag 82524, EGYPT*

<sup>c</sup>*Department of Physics, faculty of education, Ain Shams University, Roxy square EGYPT 11757, Cairo*

The dc sputtering technique was used to deposit  $\text{Al}_2\text{ZnO}_4$  thin films. X-ray diffraction (XRD) of as-prepared aluminum zinc oxide  $\text{Al}_2\text{ZnO}_4$  thin films showed that the films showed amorphous nature, whereas, the annealed films showed some crystallinity with amorphous background. The optical constants such as the refractive index  $n$ , the absorption index  $k$ , and the absorption coefficient  $\alpha$  of  $\text{Al}_2\text{ZnO}_4$  thin films were determined using spectrophotometric measurements of transmittance and reflectance in the spectral range from 200 to 1200 nm. The maximum value of the transmittance were in the range from 85% to 90% depending on the condition of preparation. Furthermore, the effect of both thickness and annealing temperature on optical energy gap  $E_{op}$ , width of the band tails of the localized states  $E_u$  plasma frequency  $\omega_p$ , and relaxation time  $\tau$  of the carriers were studied. The allowed indirect optical energy gap found to be around 3.5eV.

(Received July 12, 2012; Accepted August 28, 2012)

*Keywords:* Structural properties, Optical properties,  $\text{Al}_2\text{ZnO}_4$  thin films

### 1. Introduction

Formation and characterization of zinc oxide and doped zinc oxide via different techniques have attracted considerable attention due to their important applications in the development of materials science. ZnO has high transparency in the visible and near-ultraviolet spectral regions and a wide range of conductivity which can be changed under photo reduction/oxidation condition [1]. Pure ZnO thin films lack stability in terms of thermal aging in air and corrosive environment [2]. Thus, polycrystalline ZnO films have been doped with elements from group II and III metal ions such as In, Al, Ga, Cu Cd etc. to enhance their structural, optical and electrical properties [3-8]. Doping is required to get high transparency, stability and high conductivity. Aluminum doped ZnO thin films have high transmittance in the visible region, and low resistivity, and the optical band gap can be controlled by using Al doping amount [9]. It has been reported that the optical band gap of ZnO is approximately 3.2 eV at room temperature [4], and for  $\text{Al}_2\text{ZnO}_4$  is in the range of 3.14 - 3.32 eV [10]. This wide band gap of  $\text{Al}_2\text{ZnO}_4$  semiconductors show optical transmission in the visible and near-infrared regions. This unique property has been widely studied for various practical applications such as solar cells [11] and flat panel display electrodes [12]. In addition, it is also find applications as surface acoustic devices, optical waveguide, gas sensors, and micro-machined actuators [13-15]. The physical properties of the films depend strongly on the deposition technique, the growth conditions and post deposition treatment. Several techniques have been used for preparing ZnO thin films such as sputtering [16-17], spray pyrolysis [18], pulsed laser ablation [19], reactive evaporation [20], chemical vapor deposition [21], solution growth [22], sol-gel [23-24], and cathodic vacuum arc techniques [25].

\* Corresponding author: elneh@yahoo.com

The simultaneous occurrence of high visible transparency and high electrical conductivity can be controlled through the material parameters like dielectric constant  $\epsilon'$ , carrier concentration  $N$  and mobility [26-28].

As far as the authors know that little attention has been paid to characterizing the structural and optical properties of  $\text{Al}_2\text{ZnO}_4$  thin films deposited at room temperature. So, in the present work, the structural and optical properties of  $\text{Al}_2\text{ZnO}_4$  thin films deposited using dc sputtering technique at substrate room temperature are studied.

## 2. Experimental details

The Al doped ZnO thin films were deposited on a pre-cleaned glass substrate using UNIVEX 350 SPUTTERING UNIT with DC POWER MODEL Turbo drive TD20 classic (Leybold).and rate thickness monitor model INFICON AQM-160. The  $\text{Al}_2\text{ZnO}_4$  target, from Cathey was used as a sputtering source. The weight ratio of  $\text{Al}_2\text{O}_3$  to ZnO (both were 99.99% pure) was 20%. The high vacuum of the chamber was better than  $2 \times 10^{-6}$  torr and sputtering was carried out in an argon (99.999%) atmosphere of  $2 \times 10^{-2}$  torr. The target substrate distance was 10 cm with an angle  $65^\circ$ . The substrate temperature was kept at  $25^\circ\text{C}$  during deposition. The structural characteristics of  $\text{Al}_2\text{ZnO}_4$  thin films was investigated by X-ray diffraction pattern. Philips X-ray diffractometer model X' Pert was used for the measurements which utilized monochromatic  $\text{CuK}\alpha=1.5406 \text{ \AA}$  radiation operated at 40 kV and 25 mA. The diffraction patterns were recorded automatically with scanning speed of 2deg/min. The optical transmittance and absorbance of the films were measured in the wavelength range of 200-1200 nm at normal incidence by using double beam spectrophotometer (JASCO model V-670 UV-VIS-NIR).

## 3. Method of calculation

The study of the fundamental absorption edge provides useful complementary information concerning energy band structure and the type of transition of the charge carriers. The absorption coefficient  $\alpha$  of the films was determined using the formula [29]:

$$\alpha = \frac{1}{d} \text{Ln} \left( \frac{(1-R)^2}{T} \right) \quad (1)$$

Where  $T$  and  $R$  are the transmittance and reflectance of the films respectively and  $d$  is the film thickness.

The allowed indirect optical energy gap  $E_{op}$  was estimated from optical measurements using the following expression [30]:

$$(\alpha h\nu)^{1/2} = A(h\nu - E_{op}) \quad (2)$$

where  $h\nu$  is the photon energy,  $A$  is a constant characteristic parameter independent of photon energy, and  $h$  is Planck's constant.  $E_{op}$  values were obtained by extrapolating the linear portion of the plots of  $(\alpha h\nu)^{1/2}$  versus  $h\nu$  to  $\alpha = 0.0$ .

The refractive index  $n$  was calculated from the following equation:

$$n = \frac{1+R}{1-R} \pm \left[ \left( \frac{R+1}{R-1} \right)^2 - (1+k^2) \right]^{1/2} \quad (3)$$

where  $k = \alpha\lambda/4\pi$  is the absorption index, and  $\lambda$  the is incident wavelength. The relation between the real dielectric constant  $\varepsilon'$  and the wavelength,  $\lambda$ , in the normal dispersion region is given by [31, 32]:

$$\varepsilon' = n^2 - k^2 = \varepsilon_\infty - \frac{e^2}{4\pi^2 c^2 \varepsilon_o} \frac{N}{m^*} \lambda^2 \quad (4)$$

where  $\varepsilon_\infty$  is the residual dielectric constant,  $c$  is the light velocity,  $N$  is the free carrier concentration,  $m^*$  is the electron effective mass),  $e$  is the electronic charge and  $\varepsilon_o$  is the permittivity of free space. The plasma frequency is in the form:

$$\omega_p = \left( \frac{Ne^2}{\varepsilon_o \varepsilon_\infty m^*} \right)^{1/2} \quad (5)$$

For one kind of free carrier the relaxation time  $\tau$  can be determined by plotting  $\varepsilon'$  versus  $\lambda^2$  and calculating the slope and intercept of the straight line using the following equation:

$$\varepsilon'' = 2nk = \frac{\varepsilon_\infty \omega_p^2}{4\pi^3 c^3 \tau} \lambda^3 \quad (6)$$

where  $\varepsilon''$  is the imaginary part of the complex dielectric function. It is worth mentioning that the real part generally related to dispersion, while the imaginary part provides a measure to the dissipative rate of the wave in the medium [33]

The dispersion data of the refractive index has been analyzed on the basis of the Wemple and DiDomenico (WD) model which is based on the single oscillator formulae [34-37]:

$$(n^2 - 1)^{-1} = \frac{E_o}{E_d} - \frac{1}{E_o E_d} (h\nu)^2 \quad (7)$$

where  $E_o$  is the oscillator energy and  $E_d$  is the dispersion energy which is a measure of the strength of interband optical transition. The values of  $E_o$  and  $E_d$  can be directly determined by plotting  $(n^2 - 1)^{-1}$  against  $(h\nu)^2$ .

The amount of tailing can be estimated to a first approximation by plotting the absorption edge data in terms of an equation originally given by Urbach [38], which has been applied to many glassy materials. The exponential depends on the absorption coefficient, ( $\alpha$ ) and photon energy ( $h\nu$ ). It has been found that  $h\nu$  holds over several decades for a glassy material and takes the formula [38]

$$\alpha = \alpha_o e^{\frac{h\nu}{E_u}} \quad (8)$$

Where  $\alpha_o$  is a constant and  $E_u$  is interpreted as the width of the tail of the localized state (Urbach tails) in the forbidden band gap.

## 4. Results and discussion

### 4.1 Structural investigations

XRD of the as-prepared and annealed thin film at 200°C, 300°C and 500°C in air for 6 hrs has a crystalline nature with (004) plane preferred orientation at  $2\theta = 72.5^\circ$ , followed by amorphous background as seen in figure (1). This plane (004) has been detected at  $2\theta = 72.5^\circ$  by

Joeng et al [39]. The intensity of the peak representing the preferred plane was found to increase with increasing the annealing temperature as revealed in figure (1). This can be interpreted as due to an improvement of the crystallinity of the films.

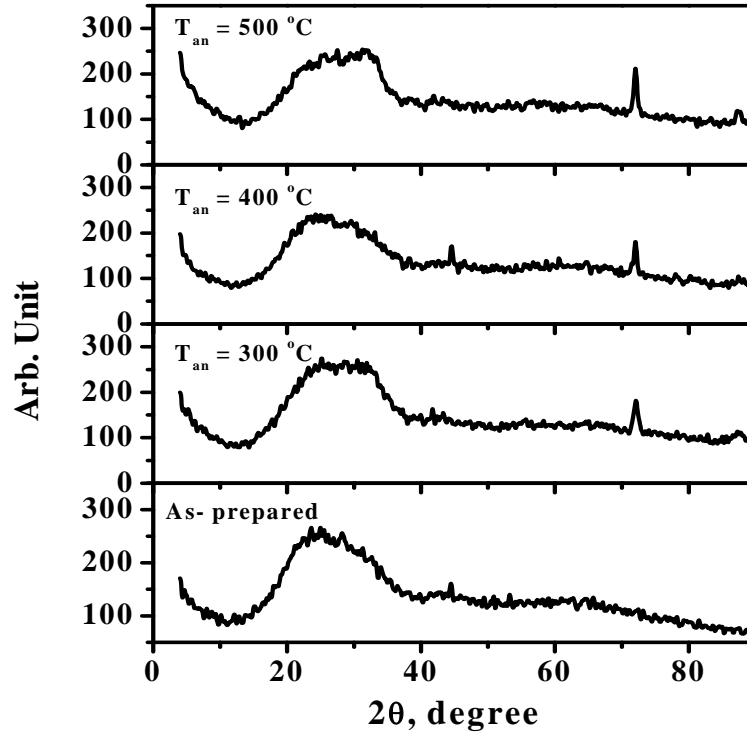


Fig. (1) : X-ray diffraction patterns of as-prepared and annealed  $Al_2ZnO_4$  thin films of 400 nm thick at 200°C, 300°C and 500°C for 6hrs.

## 4.2 Optical characterization

### 4.2.1 Effect of thickness of $Al_2ZnO_4$ thin films on the optical properties

Fig. 2 reveals the variations of transmittance with the incident wavelength. It is clear from Fig. 2 that the transmittance increases with prolongating the incident wavelength from  $\lambda = 280nm$  to  $\lambda = 600nm$  reaching maximum value of 90%, for the films with 100 and 150 nm thick respectively. Also, the transmittance of the films of thickness 200, 250 and 300 nm is 85, 77, and 75% respectively within the visible range of frequency. Increasing the incident wavelength is accompanied with a decrease in the transmittance of the thicker films reaching a lower value of 75%. The decrease in the transmittance with increasing the film thickness may be due to an increase in both reflection and absorption in the thin films. In addition, film structure may lose its homogeneity with increasing the film thickness due to accumulation of different types of structural faults, hence increasing film absorption. The transmittance loss at longer wavelengths results from photon-electron interaction, which can scatter the photons. This loss occur from both reflection and absorption. Reflection in this range is not strictly a surface phenomenon [40]. However, reflection from the bulk of the material can occur, provided that the electron escapes the surface [40]. If the scattered electron does not escape the surface, it can be concluded to have been absorbed [40]. It could be noted that at longer wavelength  $\lambda > 420nm$ , all films become transparent, whereas, at shorter wavelength  $\lambda < 420nm$  known as absorbing region is due to the existence of absorption. Figure 3 shows the relation  $(\alpha h\nu)^{1/2}$  vs.  $(h\nu)$  for as-prepared  $Al_2ZnO_4$

thin films with different thicknesses. The values of the allowed indirect optical energy gap  $E_{op}$  can be obtained from the plots of  $(\alpha h\nu)^{1/2}$  versus  $(h\nu)$  by extrapolating the linear portion of the plots of  $(\alpha h\nu)^{1/2}$  versus  $(h\nu)$  to  $\alpha = 0.0$  as shown in figure 3. The estimated values of the optical energy gap found to increase with increasing the thickness of the films as shown in table 1. This can be attributed to improvement in the crystals, in morphological changes of the films, in changes of atomic distances and grain size and structural defects in the films.

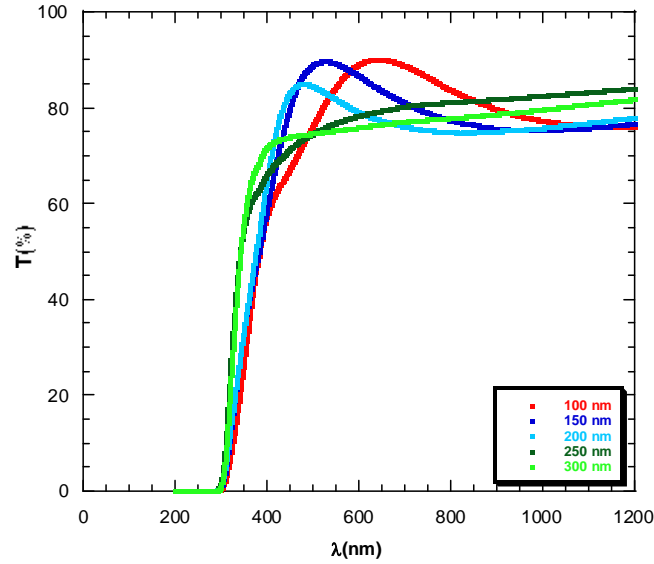


Fig.2. Variation of transmittance  $T$  with wavelength  $\lambda$  for as-prepared  $Al_2ZnO_4$  thin films of different thicknesses.

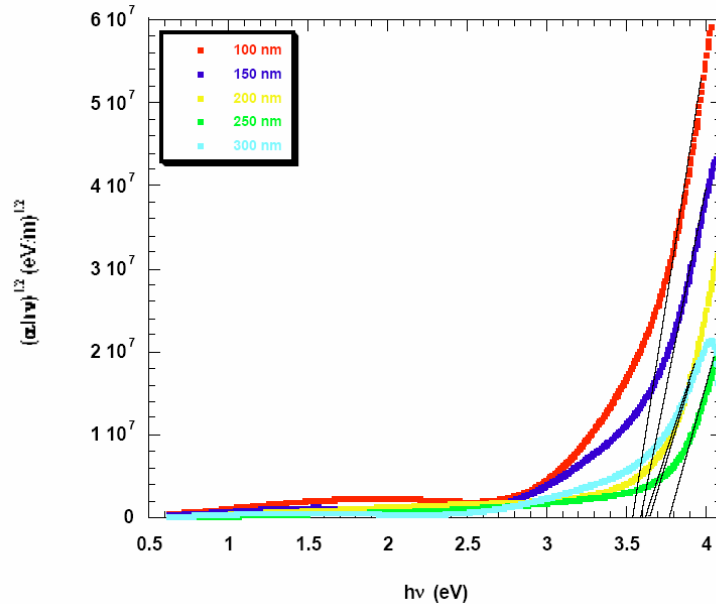


Fig. 3: Plots of  $(\alpha h\nu)^{1/2}$  vs.  $h\nu$  for as-prepared  $Al_2ZnO_4$  thin films of different thicknesses.

The width of the band tails of the localized states  $E_u$  for as-prepared  $Al_2ZnO_4$  thin films can be obtained from the slopes of the straight lines of the plot  $\ln(\alpha)$  versus  $h\nu$  as shown in Fig. 4. The values of  $E_u$  were found to have the tendency of decreasing with increasing the thickness of

the films as seen in table 1. These results of the Urbach tails confirm those of the optical energy gap.

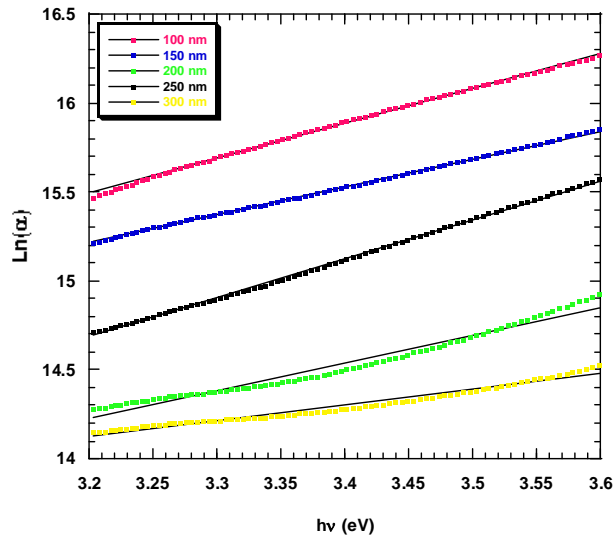


Fig. 4: Plots of  $\text{Ln}(\alpha)$  vs.  $\nu$  for as-prepared  $\text{Al}_2\text{ZnO}_4$  thin films of different thicknesses.

Fig. 5 shows the variations of the refractive index  $n$  with changing the incident wavelength. It is obvious that the refractive index decreases drastically in the range of wavelength from 450 to 700 nm for the films of thickness 200 and 250 nm. The refractive index decreases monotonically with increasing the wavelength from 800 to 2000 nm for the films with the thicknesses 150, 200, 250 and 300 nm. The decreasing of the refractive index with increasing the wavelength confirms the semiconductor behavior.

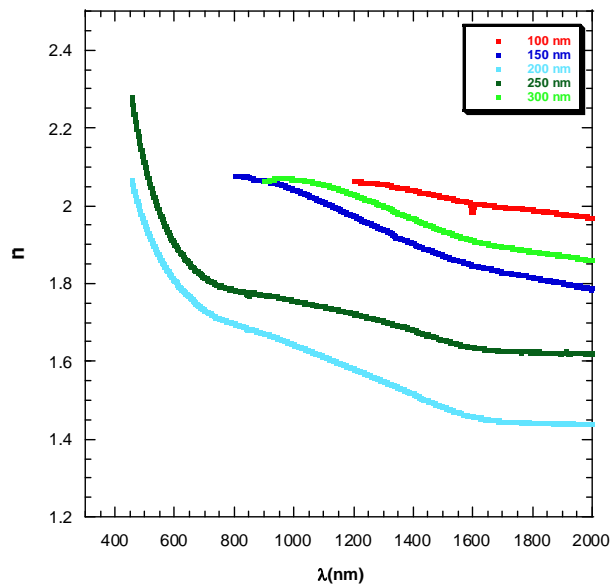


Fig. 5. Variations of the refractive index ( $n$ ) with wavelength  $\lambda$  for as-prepared  $\text{Al}_2\text{ZnO}_4$  thin films of different thicknesses.

The oscillator energy  $E_o$  and the dispersion energy  $E_d$  can be determined from the slope and intercept of the straight lines of the plot  $(n^2 - 1)^{-1}$  versus  $h\nu$  as shown in Fig.6. The values

of  $E_o$  and  $E_d$  are listed in table I. It is obvious from table I that both  $E_o$  and  $E_d$  increase with increasing the film thickness.

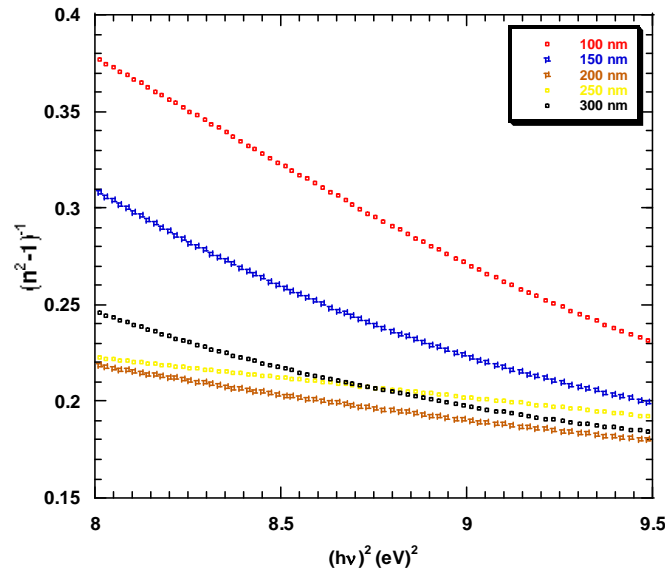


Fig. 6: Plots of  $(n^2 - 1)^{-1}$  vs.  $(h\nu)^2$  for as prepared  $Al_2ZnO_4$  thin films of different thicknesses.

The ratio of the carrier concentration  $N$  to the effective mass  $m^*$ ;  $(N/m^*)$  can be determined from the slope of the straight lines of the plots of the real part of the dielectric function  $\epsilon'$  vs.  $\lambda^2$  as seen in Fig.7. This leads to the calculation of the plasma frequency  $\omega_p$ . The values of  $(N/m^*)$  and  $\omega_p$  are listed in table I. It is found from table I that both  $(N/m^*)$  and  $\omega_p$  are decreasing with increasing the film thickness.

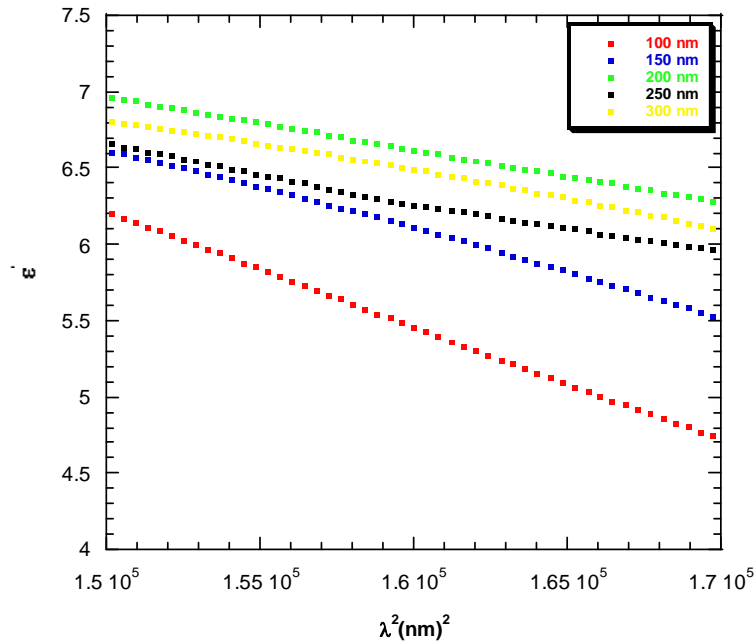


Fig. 7: Plots of dielectric constant  $\epsilon'$  with  $\lambda^2$  for as-prepared  $Al_2ZnO_4$  thin films of different thicknesses.

The relaxation time has been determined from the slope of the relation between the imaginary part of the dielectric function  $\varepsilon''$  and  $\lambda^3$  as shown in figure 8. The calculated values of the relaxation time are listed in table 1 revealing that the relaxation time increases with increasing the film thickness.

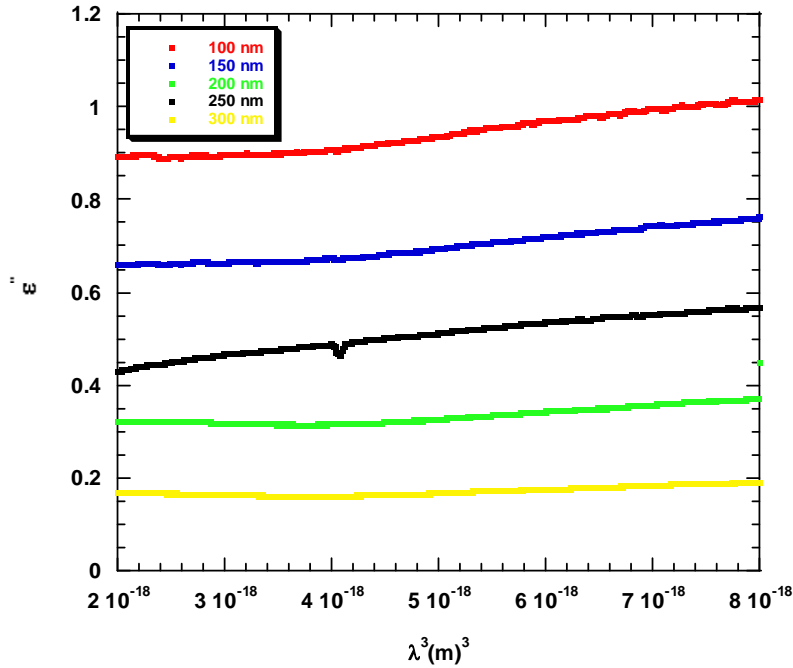


Fig. 8: Plots of  $\varepsilon''$  with  $\lambda^3$  for as-prepared  $\text{Al}_2\text{ZnO}_4$  thin films of different thicknesses.

Table 1: Optical parameters for  $\text{Al}_2\text{ZnO}_4$  thin films at different thicknesses

Film Thickness nm	$E_{op}$ (eV)	$E_u$ (eV)	$E_d$ (eV)	$E_o$ (eV)	$\varepsilon'_\infty$	$N/m^3 \times 10^{47} \text{ gm}^{-3}$	$\omega_p \times 10^{12}$ Hz	$\tau \times 10^{-14}$ S
100	3.53	0.64	2.70	0.87	3.095	2.93	5.20	1.27
150	3.60	0.55	2.97	0.92	3.071	2.15	4.5	1.32
200	3.62	0.55	3.23	1.29	3.061	1.37	3.61	1.41
250	3.65	0.58	3.47	1.42	3.078	1.37	3.59	1.44
300	3.78	0.70	3.64	1.41	3.192	1.37	3.54	1.51

#### 4.2.2 Effect of annealing temperatures on the optical properties of $\text{Al}_2\text{ZnO}_4$ thin films

Fig. 9 shows the spectral behavior of the transmittance  $T$  in the wavelength range (300-1000 nm) for as-prepared and annealed  $\text{Al}_2\text{ZnO}_4$  thin films of the same thickness 200 nm at different annealing temperature.

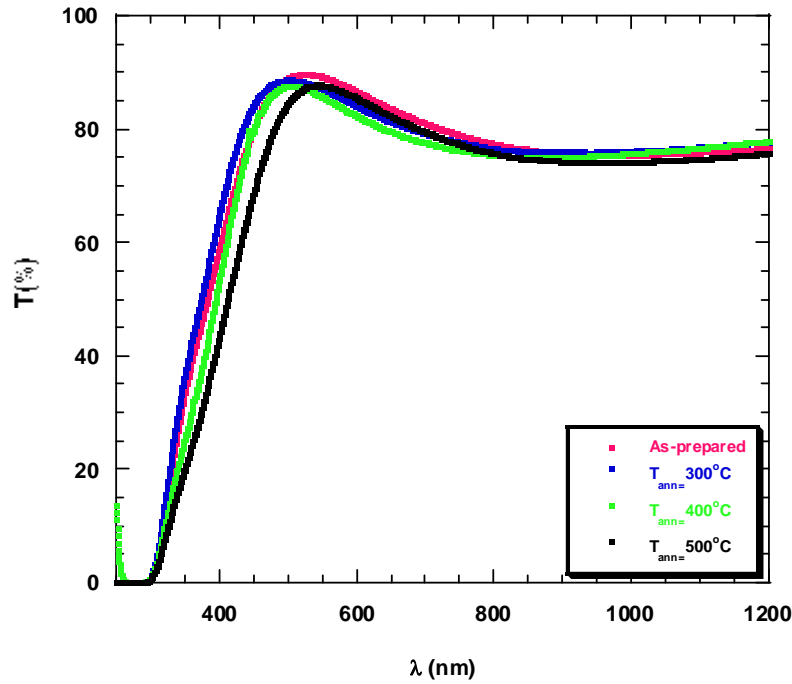


Fig. 9: Variation of transmittance  $T$  with wavelength  $\lambda$  for as-prepared and annealed  $\text{Al}_2\text{ZnO}_4$  thin films of 250 nm thick at different annealing temperature.

It is clear that annealing results in a decrease in the maximum value of the transmittance by about 2%. The decrease of transmittance with increasing annealing temperature may be due to an improvement of the degree of crystallinity of the films and/or an increase of the grain size which is confirmed by the X-ray analysis [41].

The values of the allowed indirect optical energy gap  $E_{op}$  can be obtained from the plots of  $(\alpha h\nu)^{1/2}$  versus  $(h\nu)$  by extrapolating the linear portion of the plots of  $(\alpha h\nu)^{1/2}$  versus  $(h\nu)$  to  $\alpha = 0.0$  as shown in Fig.10. The obtained values of  $E_{op}$  are listed in table 2, where  $E_{op}$  increasing with increasing the annealing temperature. This may be explained as due to quantum size effect. Also, this can be interpreted by assuming that during the annealing process the films will have time for some atomic rearrangement to take place. So, some defects will be removed which reducing the density of dangling bonds, redistributing atomic distances and bond angles and the optical gap will then increases. Some authors have observed the band gap growth phenomenon in the Al doped ZnO, but the physical origins causing such an increase are still not clarified [42]. On the other hand, physically, the band gap growth effect in Al doped ZnO system may originate from the change in the nature and strength of the interaction potentials between donors and host crystals [43]. It is generally believed that the Burstein-Moss shift plays a key role in this phenomenon [44].

The width of the band tails of the localized states  $E_u$  of as-prepared and annealed  $\text{Al}_2\text{ZnO}_4$  thin films can be calculated from the slope of the straight lines of the plots of  $\text{Ln}(\alpha)$  versus  $h\nu$  as shown in Figure 11. The calculated vales of  $E_u$  are recorded in table 2 which revealed that Urbach tails decreased with increasing the annealing temperatures. These results are consistent with those belonging to optical energy gap of the annealed films.

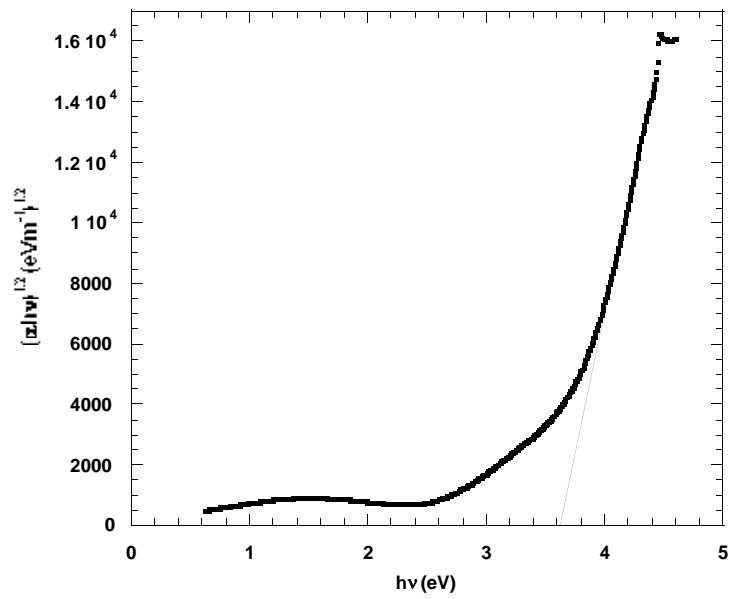


Fig.(10-a): Plots of  $(\alpha/h\nu)^{1/2}$  vs.  $h\nu$  for as-prepared  $\text{Al}_2\text{ZnO}_4$  thin film of 250 nm thick.

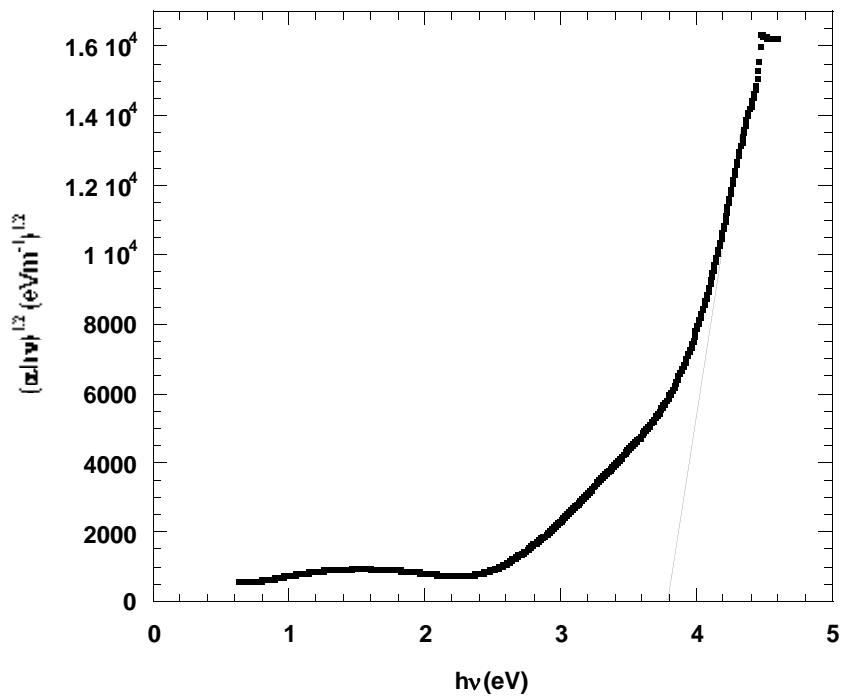


Fig.(10-b): Plots of  $(\alpha/h\nu)^{1/2}$  vs.  $h\nu$  for annealed  $\text{Al}_2\text{ZnO}_4$  thin film of 250 nm thick at 500 °C.

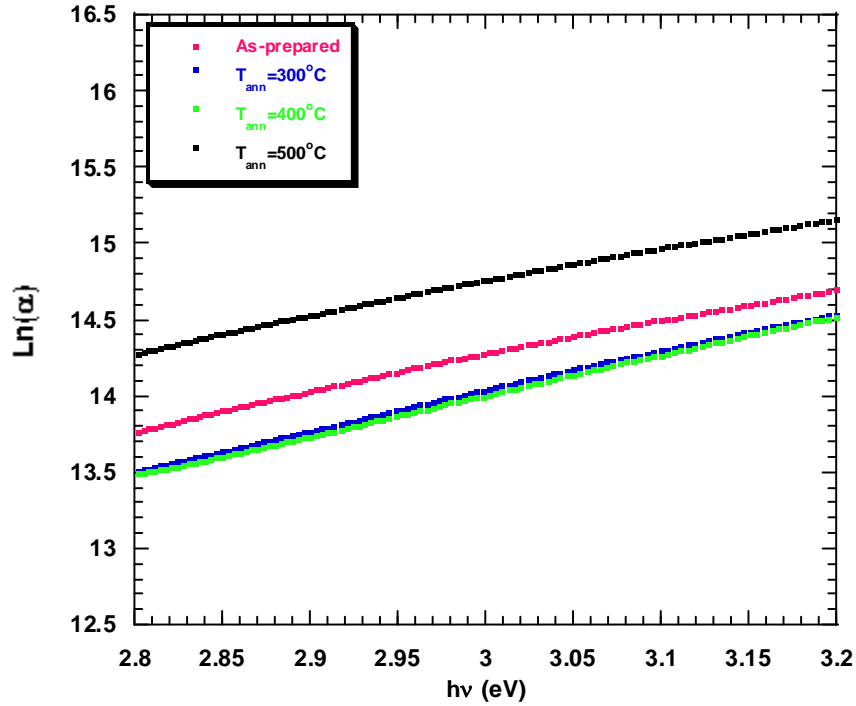


Fig. 11: Plots of  $\text{Ln}(\alpha) hv$  for as-prepared and annealed  $\text{Al}_2\text{ZnO}_4$  thin films of 250 nm thick at different annealing temperature.

The variations of refractive index in the spectral range of as-prepared and annealed  $\text{Al}_2\text{ZnO}_4$  thin films at 300 °C are shown in figure 12. The refractive index of the films decreases with annealing which can be attributed to the decrease in the packing density with increasing the annealing temperature [10].

In order to calculate the values of the single oscillator energy  $E_o$  (the average excitation energy for electronic transition) and the dispersion energy  $E_d$  (a measure of the strength of interband optical transition),  $(n^2-1)^{-1}$  is plotted against  $(h\nu)^2$  are drawn and fitted with a straight line as shown in figure 13.

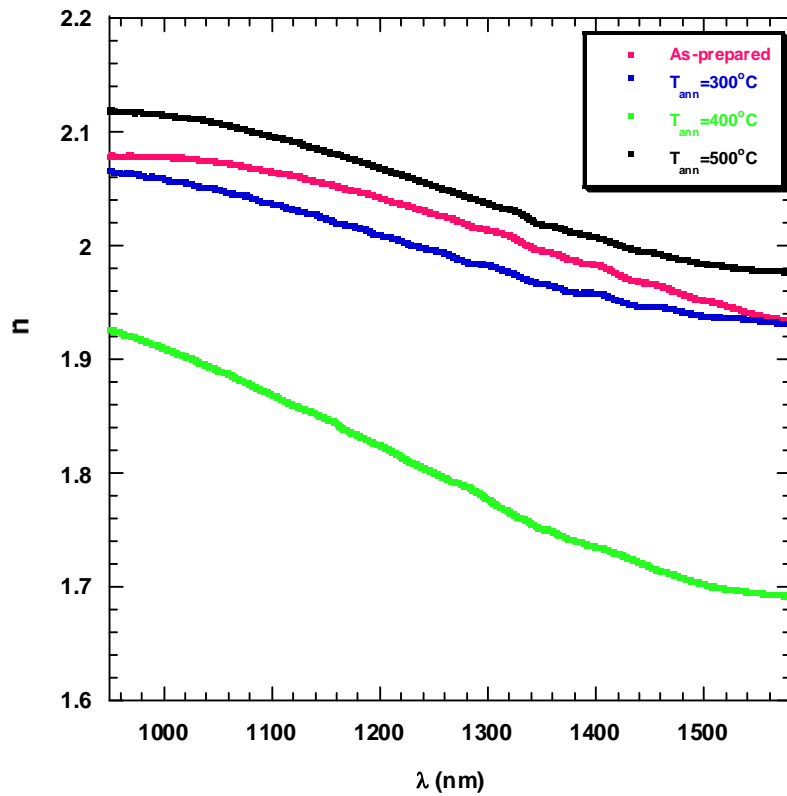


Fig. 12: Plots of refractive index  $n$  vs. wavelength  $\lambda$  for as-prepared and annealed  $\text{Al}_2\text{ZnO}_4$  thin films of 250 nm thick at different annealing temperatures.

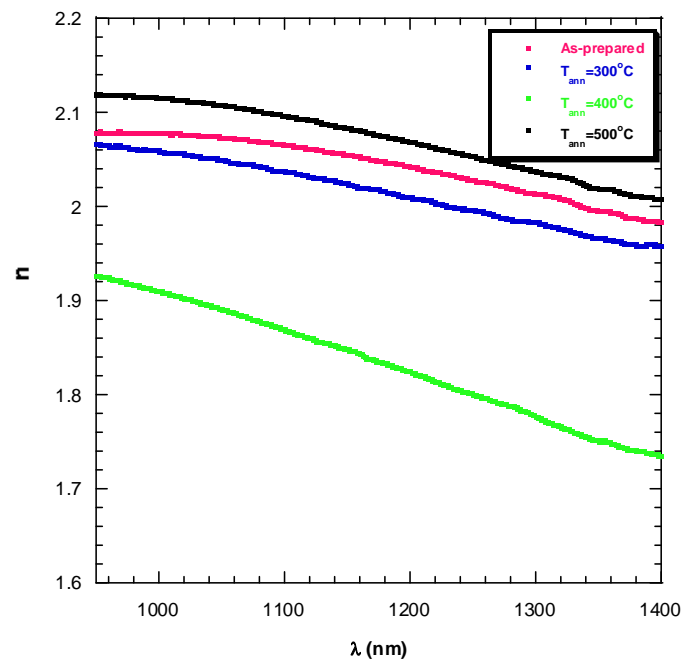


Fig. 13: Plots of refractive index  $n$  vs. wavelength  $\lambda$  for as-prepared and annealed  $\text{Al}_2\text{ZnO}_4$  thin films of 250 nm thick at different annealing temperatures.

The values of both  $E_o$  and  $E_d$  can be determined directly from the slope  $(E_o E_d)^{-1}$  and the intercept  $(E_o/E_d)$  which are listed in table 2.

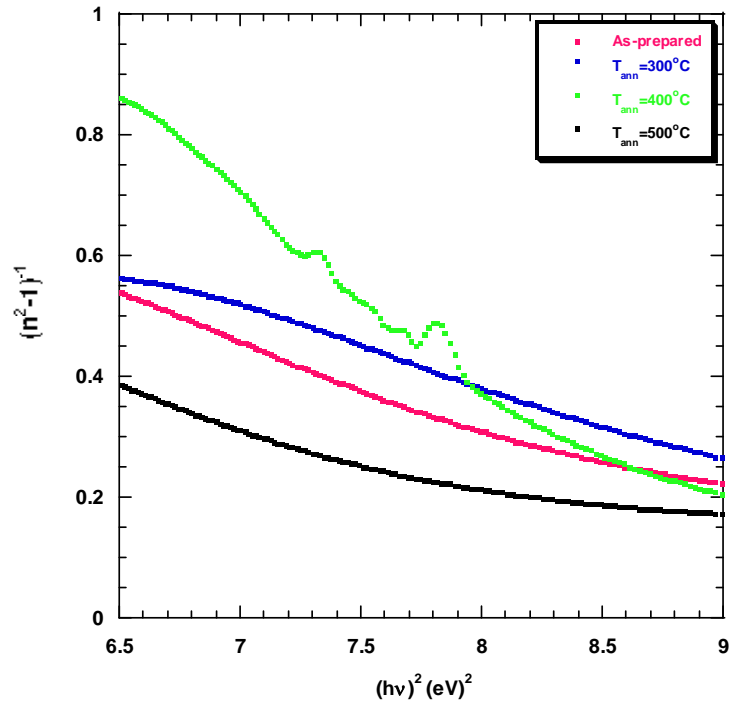


Fig. 13: Plots of  $(n^2 - 1)^{-1}$  vs.  $(hv)^2$  for as-prepared and annealed  $Al_2ZnO_4$  thin films of 250 nm thick at different annealing temperatures.

Table 2: The calculated values of allowed direct the optical energy gap  $E_{op}$  and the width of the band tails of the localized states  $E_u$ , single oscillator energy  $E_o$  and the dispersion energy  $E_d$  for as-deposited and annealed  $Al_2ZnO_4$  thin films.

Annealing temperature $^{\circ}C$	$E_{op}$ (eV)	$E_u$ (eV)	$E_o$ (eV)	$E_d$ (eV)	$N/m^* \times 10^{45}$ $gm^{-1}cm^{-3}$	$\omega_p \times 10^{14}$ Hz
As-prepared	3.62	0.67	3.15	2.01	4.85	1.71
300	3.70	0.70	3.32	2.37	4.70	1.70
400	3.75	0.62	3.01	1.01	5.20	1.74
500	3.80	0.60	3.11	2.74	5.50	1.79

It is obvious that  $E_o$  decreases with increasing annealing temperature, except for the as-prepared film. This may be due to the behavior of the optical energy gap [10]. It is clear that the dispersion energy has an opposite behavior of the single oscillator energy.

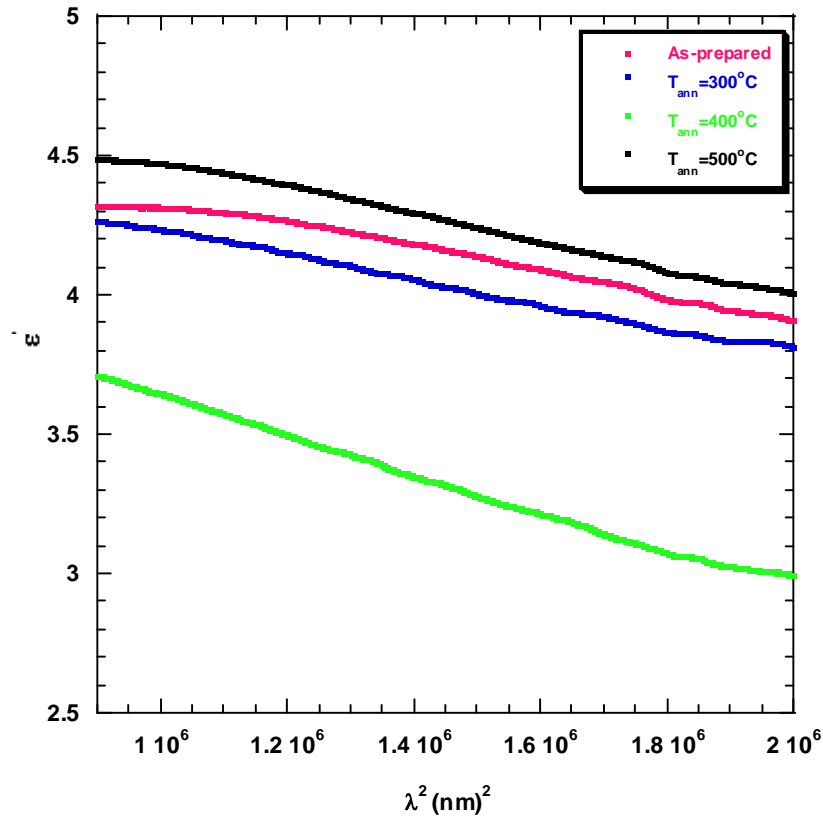


Fig. 14: Plots of dielectric constant  $\epsilon'$  vs.  $\lambda^2$  for as-prepared and annealed  $\text{Al}_2\text{ZnO}_4$  thin films of 250 nm thick at different annealing temperature.

The ratio ( $N/m^*$ ) and then the carrier concentration can be calculated from the slope the plots of  $\epsilon'$  versus  $\lambda^2$  as shown in figure 14, besides the residual dielectric constant  $\epsilon_\infty$  can be calculated from the intercept of the same plots. The values of, ( $N/m^*$ ),  $\omega_p$  and  $\epsilon_\infty$  are listed in table 2. Table 2 indicates also that  $N$  increase with annealing temperature. The increase of the carrier density  $N$  with increasing the annealing temperature is considered to be a results of the desorption of oxygen from  $\text{Al}_2\text{ZnO}_4$  film surface. Furthermore, the plasma frequency increases with increasing the temperature of annealing, which is directly proportion with the free carrier concentration. This result is in good agreement with Drude's theory.

## 5. Conclusion

It can be concluded that, the  $\text{Al}_2\text{ZnO}_4$  thin films deposited by dc sputtering showed an increase in the optical energy gap and a decrease in Urbach tails with increasing the film thickness. Whereas, dispersion energy, oscillator energy, infinite dielectric constant and relaxation time increase with increasing the thickness of the films. Besides, transmittance, the ratio ( $N/m^*$ ), and plasma frequency decrease with increasing the film thickness.

The annealed  $\text{Al}_2\text{ZnO}_4$  thin films of 250 nm thick, showed that, the optical energy gap, oscillator energy, the ratio ( $N/m^*$ ), plasma frequency increase with increasing the annealing temperature. On the other hand, Urbach tails and the dispersion energy decreases with increasing annealing temperature. Moreover, annealing results in a decrease in the transmittance by about 2%.

## References

- [1] M. Suche, S. Christoulakis, N. Katsarakis, T. Kitsopoulos and G. Kiriakidis, *Thin Solid Films* **515**, 6562 (2007).
- [2] A. E. Jimenez-Gonzalez, *Journal of Solid-State Chemistry* **28**, 176 (1997).
- [3] Y. Cao, L. Miao, S. Tanemura, M. Tanemura, Y. Kuno, Y. Hayashi and Y. Mori, *J. Appl. Phys.* **45**, 1623 (2006).
- [4] S. H. Mohamed, H. M. Ali, H. A. Mohamed, A. M. Salem, *Eur. Phys. J. Appl. Phys.* **31**, 95 (2005).
- [5] A. E. Jimenez-Gonzalez, J. A. S. Urueta, R. Suarez-Parra, *J. Cryst. Growth* **192**, 430 (1998)
- [6] W. W. Wenas, A. Yamada, A. Yamada, M. Konagai, K. Takahashi, *Jpn. J. Appl. Phys.* **30**, L441 (1991)
- [7] T. Tsuchiya, T. Emoto, T. Sei, *J. Non-Cryst. Solids* **178**, 327 (1994)
- [8] M. de la, L. Olvera, A. Maldonado, R. Asomoza, M. Mele ndez-Lira, *Sol. Energy Mater, Sol. Cells* **71**, 61 (2002)
- [9] S. H. Jeong, B. N. Park, D. G. Yoo and J. H. Boo, *Journal of Korean Physical Society* **50**, 622 (2007).
- [10] H. M. Ali, M. M. Abd El-Raheem, N. M. Megahed, H. A. Mohamed, *Journal of Physics and Chemistry of Solids* **67**, 1823 (2006).
- [11] J. A. Anna Selvan, H. keppner, A. Shah, *Mater. Res. Soc. Symp. Proc.* **426**, 497 (1996).
- [12] M. Ritala, T. Asikanen, M. Leskanen, M. LeskelaE, J. Skarp, *Mater. Res. Soc. Symp. Proc.* **426**, 513 (1996).
- [13] V. Gupta, A. Mansingh, *J. Appl. Rossi, A. Ferrari, L. S. Qian, F. Quaranta, A. Valentini, J. Mater. Res.* **5(9)**, 1929 (1990).
- [14] K.-S. Weibenrieder, J. Mueller, *Thin Solid Films* **300**, 30 (1997)
- [15] J. L. Deschanvres, B. Bochu, J. c. Joubert, *J. Phys.* **4(3)**, 485 (1993).
- [16] J. Yao, J. Lee, S. Kim, K. Yoon, I. Jun Park, S. K. Dhungel, *Thin Solid Films* **480-481**, 213 (2005).
- [17] S. Stewari, A. Bhattacharjee, *Pramana journal of physics*, **76**, 153 (2011).
- [18] J. -H Lee, B.-O. Park, *Mater. Sci. Eng. B* **106**, 242 (2004)
- [19] K. Matsubara, P. Fons, K. Iwata, A. Yamada, K. Sakurai, H. Tampo, Niki, *Thin Solid Films* **369**, 431 (2003).
- [20] J.-M. Ting, B. S. Tsai, *Mater. Chem. Phys.* **72**, 273 (2001)
- [21] C. Zhang, X. Li, J. Mian, W. yu, X. Gao, *surf Coat technol.* **198**, 253 (2005)
- [22] A. J. Varkey, A. F. Fort, *Thin Solid Films* **239**, 22 (1994)
- [23] R. Maity, S. Kundoo, K. K. Chattopadhyay, *Solar Energy Mater. Solar Cells* **86**, 217 (2005).
- [24] R. B. H. Tahar, *J. Eur. Ceram. Soc.* **25**, 3301 (2005).
- [25] H. W. Lee, S. P. Lau, Y. G. Wang, K. Y. Tse, H. H. Hng, B. K. Tay, *J. Crys. Growth* **268**, 596 (2004).
- [26] T. J. Coutts, D. L. Young, X. Li, W. P. Mulligan, X. Wu, *J. Vac. Sci. Tech. A* **18**, 2646 (2000).
- [27] K. L. Chopra, S. major, D. K. Pandya, *Thin Solid Films* **102**, 1 (1983).
- [28] R. Gordon, *MRS Bull* **25**, 52 (2000).
- [29] H. M. Ali, *Phys. Status Solidi A* **202**, 2742 (2005)
- [30] U. Pal, D. Samanta, S. Ghori, A. K. Chaudhuri, *J. Appl. Phys.* **74(10)**, 6368 (1993).
- [31] T. S. Moss, G. J. Burrell, B. Ellis, *Semiconductor optoelectronics ( Butterworths, London, 1973).*
- [32] G. A. Kumar, J. Thomas, N. George, B. A. Kumar, P. Radhakrishnan, V. P. N. Nampoori and C. P. G. Vallabhan, *Phys. Chem. Glasses*, **41(2)**, 89 (02000).
- [33] K. R. Rajesh, C. S. Menon, *Mater. Lett.* **53**, 329 (2002).
- [34] A. Abu El-Fadl, G. A. Mohamad, A. B. Abd El-Moiz, M. Rashad, *Physica B* **366**, 44 (2005)
- [35] S. Y. Kim, *Appl. Opt.* **35**, 6703 (1996).
- [36] M. M. El-Nahass, A. A. Atta, H. E. A. El-Sayed, E. F. M. El-Zaidia, *Applied Surface Science* **254**, 2458 (2008).

- [37] S. H. Wemple and DiDomenico. Rev. **B7**, 3767 (1973).
- [38] F. Urbach, Phys. Rev. **92**, 1324 (1953)
- [39] S.H. Jeong, J. W. Lee, S. B. Lee, J. H. Boo, Thin solid films, **435**, 78 (2003) -82
- [40] Robert Mamazza Jr, Don L. Morel and Christos S. Ferekides, Thin Solid Films **484**, 26 (2005).
- [41] M. M. Abd El-Raheem, H. M. Ali, N. M. El-Husainy, J. Optoelectron. Adv. Mater. **11**, 813 (2009).
- [42] M. M. Abd El-Raheem, J. Phys. Condens. Matter **19**, 216209 (2007).
- [43] Z. Q. Li, D. X. Zhang, J. J. Lin, Journal of applied Physics, **99**, 124906 (2006)
- [44] F. K. Shan and S. Yu, J. Eur. Cerm. Soc. **24**, 1869 (2004).